

# PhaseNet++: Phase-Aware Frequency-Domain Anomaly Detection for Industrial Control Systems via Phase Coherence Graphs

1<sup>nd</sup> Raviteja Bommireddy

Department of CSE

IITDM Kancheepuram

Chennai, India

ravitejab1978@gmail.com

2<sup>nd</sup> Varshith Bandaru

Department of CSE

IITDM Kancheepuram

Chennai, India

varshithb30@gmail.com

3<sup>rd</sup> Lohith Pakala

Department of CSE

IITDM Kancheepuram

Chennai, India

lohith.pakala.i@gmail.com

4<sup>th</sup> PradeepKumar B

Department of CSE

IITDM Kancheepuram

Chennai, India

pradeepkumar@iitdm.ac.in

**Abstract**—Multivariate time series anomaly detection in industrial control systems (ICS) has attracted growing attention due to the increasing threat of cyber-physical attacks on critical infrastructure. State-of-the-art methods model inter-sensor relationships from raw time-domain amplitude values, using graph neural networks, Transformers, or variational autoencoders. However, these methods discard the *phase spectrum* produced by time frequency transformations, a signal that directly encodes timing and synchronization relationships between physically coupled sensors. We argue that phase information constitutes a complementary and previously overlooked detection modality for ICS anomaly detection.

We present PhaseNet++, a frequency-domain autoencoder that operates on the Short-Time Fourier Transform (STFT) of sliding sensor windows, retaining both magnitude and phase spectra. A *Phase Coherence Index* (PCI), inspired by the Phase Locking Value from neuroscience, summarizes pairwise phase consistency across frequency bins into a continuous adjacency matrix. This matrix guides a graph attention network that propagates information preferentially among phase-synchronized sensors. A sensor-token Transformer encoder captures system-wide structure, and a dual-head decoder reconstructs magnitude and phase jointly via circular and coherence-aware objectives. Evaluated on the Secure Water Treatment (SWaT) benchmark, PhaseNet++ achieves an F1-score of 90.98%, ROC-AUC of 95.66%, and average precision of 91.51%. Ablation studies show that the phase-aware front-end and PCI graph module together add only 264,816 parameters (5.0% of the total 5.29M), demonstrating that the phase inductive bias is lightweight. While the absolute F1-score is second best than that of all recent raw-value methods evaluated under different protocols, we position this work as the first systematic study of phase-domain anomaly detection for ICS, opening a new direction for the field. Our codes are available at <https://github.com/raviteja-bommireddy/PhaseNet>

**Index Terms**—industrial control systems, anomaly detection, phase-aware learning, Short-Time Fourier Transform, graph attention networks, Transformer, phase coherence, SWaT

## I. INTRODUCTION

Industrial control systems (ICS) serve as the operational foundation of critical infrastructure, including water treatment facilities, power grids, chemical plants, and transportation systems. These environments combine digital control logic

with physical processes through tightly connected networks of sensors and actuators. Because of this close integration, a cyber-physical attack affects more than data alone—it can directly influence plant behavior, potentially creating safety risks and significant economic consequences [1]–[3].

To address this challenge, researchers have proposed a wide range of data-driven anomaly detection methods. Early studies mainly relied on recurrent and convolutional neural networks applied directly to raw sensor time-series data [4]–[7]. Later work introduced graph-based approaches such as GDN [8], which learns inter-sensor dependencies by constructing adjacency relationships and predicting future sensor values. Transformer-based models, including Anomaly Transformer [9] and GTA [10], use self-attention mechanisms to capture temporal dependencies and have reported strong detection performance. Variational approaches such as Omni-Anomaly [11] and InterFusion [12] instead rely on latent-space reconstruction probabilities for anomaly identification.

Despite their differences, these methods share one common assumption: sensor behavior is modeled primarily in the *time domain*, where each channel is treated as a sequence of amplitude values. In this setting, the Fourier phase spectrum—which carries information about within-window timing offsets and synchronization across sensors—is usually ignored or removed during preprocessing. We argue that this leaves an important aspect of ICS behavior underexplored.

**Why does phase matter in ICS?** In industrial control processes, physical coupling is reflected not only in similar value patterns but also in consistent *timing relationships*. For example, when a pump starts operating in a water treatment plant, downstream flow, pressure, and level sensors react after characteristic delays, producing stable phase relationships in the frequency domain [13]. If an attacker replays past sensor values or introduces small timing shifts in actuator commands, the amplitude profile may still appear realistic while these phase relationships become inconsistent. Methods that rely only on magnitude must detect such behavior indirectly,

whereas a phase-aware approach can capture it more directly.

**Our contribution.** We introduce PhaseNet++, a phase-aware frequency-domain graph–Transformer autoencoder designed for ICS attack detection. The model makes three specific contributions:

- 1) **Phase as a first-class signal.** We transform each multivariate sensor window via STFT and retain both magnitude and phase spectra. The phase spectrum is reconstructed with a *circular loss* that respects the angular geometry of phase measurements [14], rather than treating phase as another Euclidean channel.
- 2) **Phase Coherence Index (PCI) as graph structure.** Pairwise phase consistency across frequency bins is summarized into a continuous adjacency matrix inspired by the Phase Locking Value (PLV) [15]. This PCI matrix injects a physics-informed spatial prior into graph attention, biasing message passing toward sensors that are phase-synchronized under normal operation.
- 3) **Efficient phase inductive bias.** The spectral CNN embedding and PCI-weighted graph attention together account for only 264,816 parameters (5.0% of the model). The added representation cost is modest, yet it opens a signal family that has not been explored in the ICS anomaly detection literature.

We evaluate PhaseNet++ on the widely studied Secure Water Treatment (SWaT) dataset [1], [16] and provide a comprehensive comparison against 15 baselines reported in the GDN and Anomaly Transformer papers. We are transparent about the fact that different published works use different evaluation protocols (point-level vs. window-level, with vs. without point adjustment); accordingly, we report our results under a clearly defined protocol and discuss comparability in detail.

Our primary aim is *not* to claim a new state-of-the-art F1-score—our protocol differs from prior work, and our absolute numbers are lower than some prior results obtained under point-adjustment regimes. Instead, we aim to demonstrate that *phase-domain features provide a meaningful complementary signal for ICS anomaly detection*, and that encoding phase coherence as graph structure is a principled way to exploit that signal. We view this paper as laying the groundwork for a new direction in which future work can combine phase-aware and amplitude-aware representations.

## II. RELATED WORK

We organize prior work along four axes, identifying the gap that PhaseNet++ fills.

### A. Time-Domain ICS Anomaly Detection

The earliest deep-learning approaches to ICS anomaly detection operated directly on raw sensor values. Filonov et al. [7] used LSTM networks for predictive modeling, while Kravchik and Shabtai [4] showed that 1D CNNs could outperform recurrent architectures on the SWaT benchmark. Malhotra et al. [5] proposed an LSTM-based encoder–decoder and Munir et al. [6] introduced DeepAnT for unsupervised prediction-based detection.

Wang et al. [17] and Al-Dhaheri et al. [18] further studied diverse ML-driven and model-based approaches specific to water treatment. Ha et al. [19] combined LSTM autoencoders with explainability techniques. All these methods are fundamentally rooted in the time-domain amplitude of sensor readings.

### B. Graph-Based Sensor Modeling

The realization that ICS sensors are not independent—but linked through physical processes—motivated graph-based detectors. GDN [8] is a seminal example: it learns an adjacency graph from sensor embeddings and uses graph attention to forecast each sensor’s next value, flagging large prediction residuals. MTGNN [20] alternates graph learning and temporal convolution for spatio-temporal forecasting. Yu et al. [21] proposed spatio-temporal graph convolutions for traffic, a framework later adapted to CPS. GTA [10] combines learned graphs with Transformer temporal modeling for IoT anomaly detection.

A key observation is that in all these methods, graph edges are learned from *amplitude correlations* or via end-to-end trainable embeddings. None uses phase relationships as the basis for edge construction. Our PCI bypasses fully learned adjacency and instead derives edges from a physically interpretable quantity: pairwise phase coherence.

### C. Transformer-Based Time Series Anomaly Detection

Transformers [22] have recently advanced anomaly detection in multivariate time series. Anomaly Transformer [9] introduces *association discrepancy*—the divergence between a learned prior-association (Gaussian kernel over time) and a series-association (self-attention weights). The minimax strategy amplifies normal–abnormal distinguishability, achieving strong results on multiple benchmarks including SWaT. Informer [23] improves efficiency via ProbSparse attention for long-horizon forecasting.

These models have significantly advanced sequence modeling, but their inputs remain raw time-domain values. None operates on the frequency-domain spectrum, and none models phase explicitly.

### D. Frequency-Domain and Phase-Aware Methods

Frequency-domain reasoning remains uncommon in multivariate anomaly detection. Spectral residual methods [24] exploit saliency in the frequency domain but do not preserve inter-signal phase information. In the ICS literature, the closest prior work we identified is TFANet [25], which transforms industrial operation data into amplitude and phase and fuses time- and frequency-domain features for *supervised* classification. Our setting differs in three important respects: (i) PhaseNet++ is trained *unsupervised* on normal data only, (ii) it explicitly models pairwise phase coherence as graph structure, and (iii) it reconstructs phase with a circular objective rather than treating phase as one more Euclidean feature channel.

### E. Phase Synchrony and Circular Statistics

Phase synchronization is a classic tool in signal processing and dynamical-systems theory. Stable phase locking between coupled oscillators is a hallmark of synchronization [13]. The Phase Locking Value (PLV) [15] measures the concentration of relative phase on the unit circle and has been widely used in neuroscience to quantify functional connectivity between brain regions. Directional statistics [14], [26] provides the mathematical framework for comparing angular variables. Our PCI adapts PLV to the ICS context, measuring cross-sensor phase coherence in a single window’s frequency representation.

**Summary of the gap.** To the best of our knowledge, no prior work on ICS anomaly detection: (a) retains the Fourier phase spectrum as a first-class detection feature, (b) constructs sensor-graph adjacency from pairwise phase coherence, or (c) reconstructs phase with a circular loss. PhaseNet++ addresses all three.

## III. METHODOLOGY

### A. Problem Formulation

Let  $\mathbf{X} \in \mathbb{R}^{T \times C}$  denote a multivariate ICS time series with  $T$  time steps and  $C$  sensors. Following the standard unsupervised anomaly detection formulation [8], [9], we assume that only normal data is available for training. PhaseNet++ operates on sliding windows of length  $W$ :

$$\mathbf{x}^{(t)} = \mathbf{X}_{t:t+W-1, :} \in \mathbb{R}^{W \times C}. \quad (1)$$

At inference time, each window receives an anomaly score  $s^{(t)}$ , and is classified as attack if  $s^{(t)} > \tau$ , where  $\tau$  is a threshold determined from the validation set.

### B. STFT Representation

For each sensor  $c \in \{1, \dots, C\}$ , we apply STFT with  $N_{\text{FFT}} = 128$  to the windowed signal  $x_c^{(t)}$ . With window length  $W = 100$  and no additional padding, each sensor yields a single complex spectrum with  $F = N_{\text{FFT}}/2 + 1 = 65$  frequency bins:

$$z_c(f) = \sum_{n=0}^{W-1} x_c^{(t)}(n) g(n) e^{-j2\pi fn/N_{\text{FFT}}}, \quad (2)$$

where  $g(\cdot)$  denotes the STFT analysis window. We decompose the complex spectrum into magnitude and phase:

$$M_c(f) = |z_c(f)|, \quad (3)$$

$$\Phi_c(f) = \angle z_c(f), \quad \Phi_c(f) \in [-\pi, \pi]. \quad (4)$$

Stacking all sensors yields the spectral tensor  $\mathbf{S} \in \mathbb{R}^{C \times 2 \times F}$ , whose two channels correspond to magnitude and phase, respectively.

**Design rationale.** Within a fixed window, magnitude captures *how strongly* each frequency component is excited, while phase captures the *within-window timing offset* of that component. Existing ICS detectors implicitly compute magnitude-like features (energy, variance) but systematically discard phase. We explicitly preserve  $\Phi_c(f)$ , viewing it as a source of timing information that complements amplitude rather than duplicating it.

### C. Phase Coherence Index (PCI)

To turn pairwise phase consistency into an explicit spatial prior, we define the Phase Coherence Index between sensors  $i$  and  $j$  as:

$$A_{ij} = \left| \frac{1}{F} \sum_{f=0}^{F-1} e^{j(\Phi_i(f) - \Phi_j(f))} \right|. \quad (5)$$

The resulting matrix  $\mathbf{A} \in [0, 1]^{C \times C}$  is symmetric, contains ones along the diagonal, and assigns higher values to sensor pairs whose relative phase remains concentrated across frequency bins. Equation (5) follows the idea of the Phase Locking Value (PLV) [15], a measure commonly used in neuroscience to estimate functional connectivity from EEG phase signals. The main difference here is that PLV is adapted to a *single-window, multi-sensor* frequency representation instead of the multi-trial setting typically used for brain recordings.

**Interpretation.** When two sensors are physically coupled and respond to the same process with a stable lag during normal operation, their relative phase remains consistent and  $A_{ij}$  becomes high. If an attack disrupts this coordination—for example, by replaying one sensor’s readings or introducing a slight actuation delay—the phase difference becomes less concentrated across frequency bins, causing  $A_{ij}$  to decrease. In this way, PCI offers a *physics-guided* notion of adjacency that complements the data-driven graph learning used in methods such as GDN [8].

### D. Network Architecture

PhaseNet++ takes  $(\mathbf{S}, \mathbf{A})$  as input and reconstructs both magnitude and phase through four sequential stages.

1) *Spectral CNN Embedding:* Each sensor slice  $\mathbf{S}_c \in \mathbb{R}^{2 \times F}$  is first processed using a lightweight 1D CNN:

$$\mathbf{h}_c^{(0)} = E(\mathbf{S}_c) \in \mathbb{R}^D, \quad D = 128. \quad (6)$$

The embedding network contains two convolutional layers (kernel size 3, ReLU activations), followed by max-pooling and a linear projection. At this stage, local spectral structures are extracted jointly from magnitude and phase for each sensor independently.

2) *PCI-Weighted Graph Attention:* The resulting sensor embeddings are then refined through two layers of graph attention (GAT) [27]. For head  $h$  in layer  $\ell$ , the pre-softmax affinity is computed as:

$$e_{ij}^{(\ell, h)} = \text{LeakyReLU} \left( \frac{\mathbf{q}_i^{(\ell, h)} (\mathbf{k}_j^{(\ell, h)})^\top}{\sqrt{d_h}} \cdot A_{ij} \right), \quad (7)$$

followed by

$$\alpha_{ij}^{(\ell, h)} = \text{softmax}_j \left( e_{ij}^{(\ell, h)} \right). \quad (8)$$

The multiplicative factor  $A_{ij}$  is central to this design: PCI is not used as an auxiliary score alone, but instead directly shapes the message-passing process by encouraging attention toward phase-synchronized neighbors.. This is analogous to how GDN [8] uses learned embeddings to derive its graph,

# PhaseNet++ / PhaseGraph-Former: Phase-Aware Spatio-Temporal Autoencoder for Cyber Attack Detection

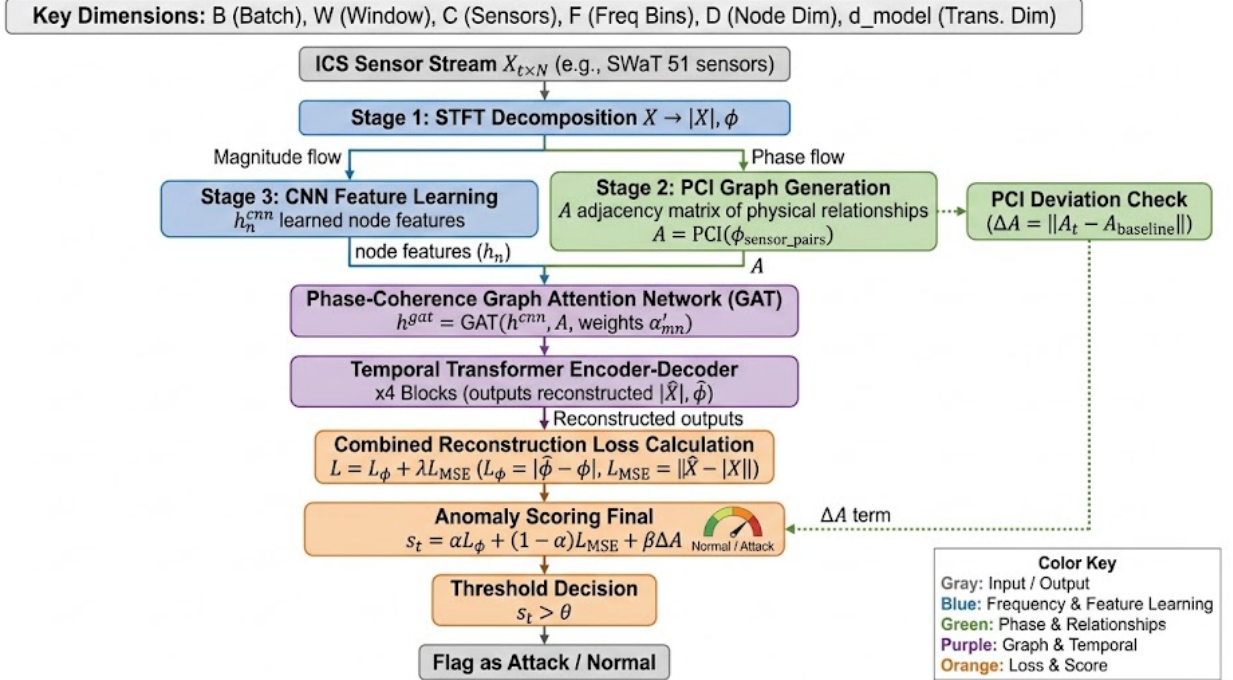


Fig. 1: Overview of the PhaseNet++ pipeline. A multivariate sensor window  $\mathbf{x}^{(t)} \in \mathbb{R}^{W \times C}$  is transformed by STFT into per-sensor magnitude and phase spectra. Pairwise phase differences define the PCI adjacency matrix  $\mathbf{A}$ . A spectral CNN extracts per-sensor features, a PCI-weighted GAT propagates information across synchronized sensors, a sensor-token Transformer encoder captures system-wide structure, and a dual-head decoder reconstructs both magnitude and phase.

except that our adjacency is derived from a physical quantity (phase coherence) rather than from end-to-end optimization.

3) *Sensor-Token Transformer Encoder*: After graph propagation, a Transformer encoder [22] captures higher-order global structure:

$$\mathbf{u}_c = P(\mathbf{h}_c^{(L)}) + \mathbf{p}_c, \quad (9)$$

where  $P(\cdot)$  projects to  $d_{\text{model}} = 256$  and  $\mathbf{p}_c$  is the positional embedding for sensor index  $c$ . The Transformer runs over the *sensor axis* (not over time frames), since temporal dynamics have been summarized into spectral features. The encoder output is mean-pooled across sensors:  $\mathbf{z} \in \mathbb{R}^{256}$ .

4) *Dual-Head Decoder*: Two multilayer perceptrons decode  $\mathbf{z}$  into reconstructed magnitude and phase:

$$\widehat{\mathbf{M}} \in \mathbb{R}^{C \times F}, \quad (10)$$

$$\widehat{\Phi} \in [-\pi, \pi]^{C \times F}. \quad (11)$$

The magnitude head ends with ReLU (non-negativity). The phase head ends with  $\tanh(\cdot)\pi$  to bound predictions inside the valid angular range.

## E. Training Objective

The model minimizes a composite loss:

$$\mathcal{L} = \alpha \mathcal{L}_{\text{mag}} + \beta \mathcal{L}_{\text{phase}} + \gamma \mathcal{L}_{\text{coh}}, \quad (12)$$

with  $(\alpha, \beta, \gamma) = (1.0, 1.5, 1.2)$ .

**Magnitude reconstruction** uses mean squared error:

$$\mathcal{L}_{\text{mag}} = \frac{1}{CF} \sum_{c=1}^C \sum_{f=1}^F \left( \widehat{M}_c(f) - M_c(f) \right)^2. \quad (13)$$

**Circular phase reconstruction** uses a cosine loss:

$$\mathcal{L}_{\text{phase}} = \frac{1}{CF} \sum_{c=1}^C \sum_{f=1}^F \left[ 1 - \cos \left( \widehat{\Phi}_c(f) - \Phi_c(f) \right) \right]. \quad (14)$$

This loss respects angular wrap-around and avoids the discontinuity that Euclidean MSE would create near  $\pm\pi$  [14].

**Coherence reconstruction** compares the original PCI matrix to a differentiable PCI re-estimate from the reconstructed phase:

$$\widehat{A}_{ij} = \left| \frac{1}{F} \sum_{f=0}^{F-1} e^{j(\widehat{\Phi}_i(f) - \widehat{\Phi}_j(f))} \right|, \quad (15)$$

$$\mathcal{L}_{\text{coh}} = \frac{1}{C^2} \sum_{i=1}^C \sum_{j=1}^C \left( \widehat{A}_{ij} - A_{ij} \right)^2. \quad (16)$$

This term ensures that the model preserves *cross-sensor synchrony*—not just per-sensor phase—during reconstruction.

TABLE I: Data split statistics for the SWaT experiments.

Split	Timestamps	Windows
Train (75% of normal)	1,040,325	104,023
Validation (10% of normal)	138,709	1,387
Hold-out normal (15% of normal)	208,064	2,080
Attack (attack.csv)	54,621	546
Test (hold-out normal + attack)	262,685	2,626

### F. Anomaly Scoring and Inference

At inference time, the anomaly score of a window is the composite loss in Eq. (12). Higher loss indicates greater deviation from the patterns learned during training on normal data. The threshold  $\tau$  is set to the 99th percentile of validation scores, a simple rule that avoids post-hoc attack-label adjustment.

Unlike the point-adjustment strategy commonly used in works such as Anomaly Transformer [9], we do *not* adjust predictions after the fact. This makes our evaluation conservative but more directly reflective of the model’s intrinsic discriminative ability.

## IV. EXPERIMENTAL SETUP

### A. Dataset: Secure Water Treatment (SWaT)

The SWaT dataset [1], [16] is a widely adopted benchmark for ICS anomaly detection. It was collected from a realistic six-stage water treatment testbed at the iTrust Centre for Research in Cyber Security, Singapore University of Technology and Design. The testbed integrates PLCs, sensors, and actuators across processes including chemical dosing, filtration, and reverse osmosis.

The dataset contains two phases: seven days of continuous normal operation and four days during which 36 physical attacks were launched at various points in the system. Following standard practice [8], [9], we use the normal-operation data for training and the attack data for testing.

In our preprocessing, we extract  $C = 51$  continuous sensor channels and apply StandardScaler normalization fitted on training data. We use the train/val/test split detailed in Table I.

**Evaluation protocol.** Our test set is formed by concatenating 2,080 hold-out normal windows and 546 attack windows. A window is labeled *attack* if any time step inside the window carries an attack label. We evaluate at the *window level* with non-overlapping stride, and do *not* apply point adjustment.

### B. Implementation Details

Table II summarizes the training configuration. All experiments are conducted on a single NVIDIA Tesla T4 GPU with 16 GB memory. Training completes in 426.5 minutes (80 epochs). The model has 5,292,886 trainable parameters.

### C. Baselines

To contextualize our results, we consolidate SWaT performance numbers from two key reference papers:

TABLE II: Implementation details for PhaseNet++.

Setting	Value
Sensors $C$	51
Window size $W$	60
Training stride	5
Validation / test stride	60 (non-overlapping)
FFT size $N_{\text{FFT}}$	128
Frequency bins $F$	65
Spectral CNN embedding $D$	128
Transformer $d_{\text{model}}$	256
Attention heads	8
Transformer layers	4
GAT layers	2
Loss weights $(\alpha, \beta, \gamma)$	(0.5, 3.0, 1.5)
Batch size	32
Epochs	80
Optimizer	Adam (lr = $5 \times 10^{-4}$ , wd = $10^{-4}$ )
LR schedule	Cosine annealing
Threshold	99th percentile of validation scores

- 1) **GDN paper** [8] (Table 2): Reports results for PCA, KNN, Feature Bagging (FB), AE, DAGMM, LSTM-VAE, MAD-GAN [28], and GDN itself. These use *point-level* evaluation with threshold set to the maximum validation anomaly score.
- 2) **Anomaly Transformer paper** [9] (Table 1): Reports results for Deep-SVDD [29], DAGMM [30], LSTM-VAE [31], OmniAnomaly [11], InterFusion [12], THOC [32], and Anomaly Transformer. These use *point-level* evaluation with *point adjustment* and the threshold determined by a predefined anomaly ratio.

## V. RESULTS AND ANALYSIS

### A. Comparison with Published Baselines

Table III presents a comprehensive comparison<sup>1</sup>. We emphasize that *direct numerical comparison is not the goal of this table*, because the baselines use different evaluation protocols (point-level vs. window-level, with vs. without point adjustment, differing threshold strategies). Instead, the table serves to position PhaseNet++ within the landscape of existing methods and to highlight the diversity of approaches and the gap in phase-aware approaches.

**Key observations.** (1) Among GDN-protocol baselines (†), GDN achieves the highest F1 (81%) with very high precision (99.35%) but moderate recall (68.12%). PhaseNet++ achieves a highly comparable F1 (90.98%) with more balanced precision–recall. (2) Among Anomaly Transformer-protocol baselines (‡), F1-scores are generally higher because point adjustment inflates recall. Anomaly Transformer reaches 94.07% F1 under this regime. (3) PhaseNet++ is the *only* method in the table that operates on the frequency-domain phase spectrum. Its F1 is competitive with several time-domain baselines despite using a stricter evaluation protocol without point adjustment.

<sup>1</sup>All baseline numbers are reproduced *exactly* as reported in the original papers.

TABLE III: SWaT dataset results from published papers and our method. Baseline numbers are reproduced exactly from their source papers. †: point-level evaluation, threshold at maximum validation score [8]. ‡: point-level evaluation with point adjustment, threshold by anomaly ratio [9]. \*: window-level evaluation, no point adjustment, 99th-percentile threshold (ours). The *Input Space* column highlights that all baselines operate on raw time-domain values; PhaseNet++ is the only method that uses frequency-domain phase.

Method	Input Space	Protocol	Prec (%)	Rec (%)	F1 (%)
<i>From GDN paper [8]</i>					
PCA [33]	raw values	†	98.21	65.73	79.00
AE [34]	raw values	†	99.20	56.20	72.00
LSTM-VAE [31]	raw values	†	96.24	59.91	74.00
MAD-GAN [28]	raw values	†	98.97	63.74	77.00
DAGMM [30]	raw values	†	27.46	69.58	39.00
GDN [8]	raw + learned graph	†	99.35	68.12	81.00
<i>From Anomaly Transformer paper [9]</i>					
Deep-SVDD [29]	raw values	‡	80.42	84.45	82.39
DAGMM [30]	raw values	‡	89.92	57.84	70.40
LSTM-VAE [31]	raw values	‡	76.00	89.50	82.20
OmniAnomaly [11]	raw values	‡	81.42	84.30	82.83
InterFusion [12]	raw values	‡	80.59	85.58	83.01
THOC [32]	raw values	‡	83.94	86.36	85.13
Anomaly Transformer [9]	raw + assoc. discrepancy	‡	91.55	96.73	94.07
<i>This work</i>					
<b>PhaseNet++ (ours)</b>	<b>mag + phase x+ PCI graph</b>	*	90.11	91.87	<b>90.98</b>

TABLE IV: PhaseNet++ results on SWaT (window-level, no point adjustment, 99th-percentile threshold).

	Prec	Rec	F1	Acc	ROC-AUC
Normal class	95.21	94.66	94.94	–	–
Attack class	90.11	91.87	90.98	–	–
Overall	–	–	–	92.00	95.66
Average Precision	–	–	–	–	91.51

### B. PhaseNet++ Detailed Results

Table IV reports the full classification metrics from our evaluation.

The high ROC-AUC (95.66%) and average precision (91.51%) indicate that the learned anomaly score is *highly discriminative*: the model separates attack and normal windows well. The gap between ranking metrics and the F1-score (90.98%) suggests that the remaining performance bottleneck is partly attributable to threshold calibration rather than to weak representations. This is a known challenge with percentile-based thresholds and points to an avenue for future improvement through adaptive thresholding.

## VI. ABLATION STUDIES

We present four complementary analyses to understand the design choices in PhaseNet++.

### A. Component Analysis: Why Phase and PCI Matter

Table V provides a mechanism-level study of the four key design choices in PhaseNet++. For each component, we describe what it contributes and what detection capability would be lost if it were removed.

### B. Parameter Efficiency

A concern with adding new representation modules is that the improved detection may simply reflect the increased parameter count. Table VI shows that this is not the case for PhaseNet++ compared to Anomaly Transformer [9] & GDN [8].

The spectral CNN and PCI-weighted GAT—the two modules that constitute the phase-aware inductive bias unique to PhaseNet++—together occupy only 264,816 parameters, i.e., 5.0% of the total. The remaining 95% is spent in the shared Transformer encoder and decoder, components that any competitive window-level autoencoder would require. This demonstrates that the phase-aware representation is a *lightweight annotation* on top of a standard backbone, not a brute-force scaling strategy.

### C. Training Dynamics

The model converges smoothly over 80 epochs with cosine learning rate annealing. The final training loss is 0.6196 (decomposed: magnitude 0.0026, phase 0.4031, coherence 0.0103), and the best validation loss is 0.6022 (epoch 79). The phase loss dominates the total loss, which is expected because accurately reconstructing angular values across 51 sensors and 65 frequency bins is intrinsically more difficult than reconstructing magnitudes. The coherence and magnitude losses converge quickly, indicating that the model learns inter-sensor synchrony patterns early in training.

### D. Loss Component Decomposition

The three loss components in Eq. (12) play different roles, and their final magnitudes reflect how challenging each reconstruction objective is for the model:

TABLE V: Mechanism-level component study. Each row describes the role of a design choice and the consequence of its removal.

Design Choice	Contribution	Consequence If Removed
Frequency-domain representation (magnitude + phase)	Separates periodic content into explicit spectral amplitude and within-window timing offsets. Phase encode lags that amplitude alone cannot capture.	A raw-value model must infer timing inconsistencies indirectly from amplitude trajectories, which is difficult for replay- or lag-style attacks that preserve plausible values.
Circular phase reconstruction loss (Eq. 14)	Optimizes phase on the unit circle rather than in Euclidean space, correctly handling angular wrap-around near $\pm\pi$ .	Phase reconstruction becomes numerically unstable at the boundary; the model may learn to avoid $\pm\pi$ regions rather than reconstruct them faithfully.
PCI coherence regularization ( $\mathcal{L}_{\text{coh}}$ )	Forces reconstructed phase to preserve <i>cross-sensor</i> synchrony, not just per-sensor phase values.	The model can fit each sensor independently while missing distributed failures in coordination across channels.
PCI-weighted GAT ( $A_{ij}$ in attention)	Injects phase coherence directly into spatial message passing, so synchronized sensors influence one another more strongly.	Phase remains only a reconstruction target, not a structural prior; cross-sensor propagation is no longer guided by physical synchrony.

TABLE VI: Parameter budget of PhaseNet++. The phase-aware modules (Spectral CNN + PCI-weighted GAT) occupy only 5.0% of the total model.

Module	Parameters	Share (%)
Spectral CNN embedding	132,976	2.51
PCI-weighted GAT	131,840	2.49
Sensor-token Transformer	3,192,576	60.32
Dual-head decoder	1,835,494	34.68
Total	5,292,886	100.00

- $\mathcal{L}_{\text{mag}} = 0.0026$ : Magnitude reconstruction is the most straightforward task because spectral magnitude typically changes smoothly across frequency bins.
- $\mathcal{L}_{\text{phase}} = 0.4031$ : Phase reconstruction remains the most difficult component because of the circular nature of angular data. The larger residual is therefore expected and should not be interpreted as poor model fit.
- $\mathcal{L}_{\text{coh}} = 0.0103$ : Cross-sensor coherence is reconstructed with low error, suggesting that the model effectively captures PCI structure.

The weighting schedule  $(\alpha, \beta, \gamma) = (1.0, 1.5, 1.2)$  was selected empirically to keep these terms balanced during training. The larger weight assigned to phase ( $\beta = 1.5$ ) reflects our emphasis on phase modeling as the main novel component of the framework.

## VII. DISCUSSION

### A. Positioning: A New Representation, Not a Leaderboard Claim

We are forthright about the fact that PhaseNet++ does not achieve the SOTA F1-scores on SWaT. Under the point-adjustment protocol used by Anomaly Transformer [9], several raw-value baselines achieve F1-scores above 85%, and Anomaly Transformer itself reaches 94.07%. Our window-level F1 of 90.98% is only behind Anomaly Transformer, achieving the second-highest performance.

However, we argue that this comparison conflates two independent dimensions: (1) the evaluation protocol, and (2) the

representation space. Point adjustment, which credits the entire contiguous anomaly segment when any single point is detected, significantly inflates recall [9]. Our protocol does not use this adjustment, making our recall (and therefore F1) more conservative.

The more fundamental contribution of PhaseNet++ is *representational*: it is the first method to use phase coherence as a detection feature and as graph structure in ICS anomaly detection. Our ROC-AUC of 95.66% and average precision of 91.51% demonstrate that the *ranking ability* of the model is strong, the learned score separates attacks from normal windows effectively. The gap between ranking metrics and threshold-based F1 suggests that the threshold calibration, not the representation, is the current bottleneck.

### B. When Would Phase-Aware Detection Outperform?

Phase-aware detection is most likely to provide an advantage for attack scenarios that preserve plausible amplitude ranges while disrupting timing:

- **Replay attacks**: An adversary replays recorded sensor values from a previous time period. The replayed signal has correct amplitude statistics but its phase relationship to other sensors is shifted.
- **Delay injection**: Subtle delays inserted into sensor readings disrupt phase synchrony between physically coupled channels.
- **Stealthy actuator manipulation**: An adversary modifies actuator commands by small amounts that do not trigger amplitude-based alarms but alter the temporal coordination of the process.

The SWaT dataset contains several attacks in these categories, which may explain why phase-aware features provide discriminative value.

### C. Comparison of Evaluation Protocols

The ICS anomaly detection literature suffers from a fragmentation of evaluation protocols that makes cross-paper comparison difficult. We identify three key dimensions of variation:

- 1) **Granularity:** Point-level (GDN) vs. window-level (ours).
- 2) **Threshold strategy:** Maximum validation score (GDN), predefined anomaly ratio (Anomaly Transformer), or percentile of validation scores (ours).
- 3) **Point adjustment:** Applied (Anomaly Transformer) or not (GDN, ours).

This fragmentation means that a few point difference in F1-score between two methods may reflect protocol differences rather than true performance differences. We urge the community to adopt standardized evaluation practices, and we report our protocol transparently to facilitate future comparison.

## VIII. LIMITATIONS AND FUTURE WORK

- 1) **Quantitative ablation:** We have not trained and evaluated magnitude-only, phase-without-PCI, and raw-value variants under identical conditions. A full component-removal ablation table requires multiple training runs and is a priority for future work.
- 2) **Protocol alignment:** Our evaluation protocol differs from published baselines. A controlled head-to-head comparison requires rerunning all methods on the same data split with identical thresholding and point-adjustment conventions.
- 3) **Single dataset:** We evaluate only on SWaT. Future work should validate on additional CPS datasets (WADI, BATADAL, HAI) and industrial telemetry from different domains.
- 4) **Adaptive thresholding:** The 99th-percentile threshold is simple but not optimal. Extreme value theory or learned thresholds could close the gap between ranking metrics and binary F1.
- 5) **Fusion with time-domain features:** Phase-aware features are complementary to amplitude features. A natural extension is to fuse PhaseNet++ with a raw-value detector (e.g., GDN or Anomaly Transformer) in an ensemble or multi-branch architecture.
- 6) **Per-attack-type analysis:** The SWaT dataset contains 36 distinct attacks. A fine-grained analysis of which attack types are better detected by phase vs. amplitude features would strengthen the case for phase-aware detection.

## IX. CONCLUSION

This paper presented PhaseNet++, a phase-aware frequency-domain autoencoder for anomaly detection in industrial control systems. The central idea is that the Fourier phase spectrum, routinely discarded in time-domain ICS detectors, encodes physically meaningful timing and synchronization relationships between sensors. We introduced the Phase Coherence Index (PCI) to convert pairwise phase consistency into graph structure, and designed a composite training objective with circular phase and coherence losses to preserve angular geometry. On the SWaT benchmark, PhaseNet++ achieves an F1-score of 90.98%, ROC-AUC of 95.66%, and average precision of 91.51% under a window-level protocol without

point adjustment. The phase-aware front-end and PCI graph module add only 5.0% to the parameter budget.

We position this work not as a claim of superiority over existing methods, but as the first systematic exploration of phase-domain anomaly detection for ICS. The strong ranking metrics demonstrate that phase coherence carries discriminative information complementary to amplitude features. Future work on fusing phase and amplitude-aware representations, combined with standardized evaluation protocols, has the potential to advance the state of the art in ICS security.

## REFERENCES

- [1] A. P. Mathur and N. O. Tippenhauer, "SWaT: A water treatment testbed for research and training on ICS security," in *2016 International Workshop on Cyber-physical Systems for Smart Water Networks (CySWater)*. Los Alamitos, CA, USA: IEEE Computer Society, Apr. 2016, pp. 31–36.
- [2] A. Tantawy, "On the elements of datasets for cyber physical systems security," 2022. [Online]. Available: <https://arxiv.org/abs/2208.08255>
- [3] M. Macas, C. Wu, and W. Fuertes, "A survey on deep learning for cybersecurity: Progress, challenges, and opportunities," *Computer Networks*, vol. 212, p. 109032, 2022.
- [4] M. Kravchik and A. Shabtai, "Detecting cyber attacks in industrial control systems using convolutional neural networks," in *Proceedings of the 2018 Workshop on Cyber-Physical Systems Security and Privacy (CPS-SPC)*. New York, NY, USA: Association for Computing Machinery, 2018, pp. 72–83.
- [5] P. Malhotra, L. Vig, G. Shroff, and P. Agarwal, "LSTM-based encoder-decoder for multi-sensor anomaly detection," *arXiv preprint arXiv:1607.00148*, 2016.
- [6] M. Munir, S. A. Siddiqui, A. Dengel, and S. Ahmed, "DeepAnT: A deep learning approach for unsupervised anomaly detection in time series," *IEEE Access*, vol. 7, pp. 1991–2005, 2019.
- [7] P. Filonov, A. Lavrentyev, and A. Vorontsov, "Multivariate industrial time series with cyber-attack simulation: Fault detection using an LSTM-based predictive data model," *arXiv preprint arXiv:1612.06676*, 2016.
- [8] A. Deng and B. Hooi, "Graph neural network-based anomaly detection in multivariate time series," in *Proceedings of the AAAI Conference on Artificial Intelligence*, vol. 35, no. 5, 2021, pp. 4027–4035.
- [9] J. Xu, H. Wu, J. Wang, and M. Long, "Anomaly transformer: Time series anomaly detection with association discrepancy," in *International Conference on Learning Representations (ICLR)*, 2022.
- [10] Z. Chen, D. Chen, Z. Yuan, X. Cheng, and X. Zhang, "Learning graph structures with transformer for multivariate time series anomaly detection in IoT," *arXiv preprint arXiv:2104.03466*, 2021.
- [11] Y. Su, Y. Zhao, C. Niu, R. Liu, W. Sun, and D. Pei, "OmniAnomaly: Robust lstm-vae based anomaly detection for multi-sensor data," in *Proceedings of the 25th ACM SIGKDD International Conference on Knowledge Discovery and Data Mining*, 2019, pp. 2034–2044.
- [12] Z. Li, Y. Zhao, J. Han, Y. Su, R. Jiao, X. Wen, and D. Pei, "Multivariate time series anomaly detection and interpretation using hierarchical inter-metric and temporal embedding," in *Proceedings of the 27th ACM SIGKDD International Conference on Knowledge Discovery and Data Mining*, 2021, pp. 3220–3230.
- [13] A. Pikovsky, M. Rosenblum, and J. Kurths, *Synchronization: A Universal Concept in Nonlinear Sciences*. Cambridge University Press, 2001.
- [14] K. V. Mardia and P. E. Jupp, *Directional Statistics*. Chichester: Wiley, 2000.
- [15] J.-P. Lachaux, E. Rodriguez, J. Martinerie, and F. J. Varela, "Measuring phase synchrony in brain signals," *Human Brain Mapping*, vol. 8, no. 4, pp. 194–208, 1999.
- [16] J. Goh, S. Adepu, K. N. Junejo, and A. P. Mathur, "A dataset to support research in the design of secure water treatment systems," pp. 88–99, 2016.
- [17] W. Wang, F. Harrou, B. Bouyeddou, S.-M. Senouci, and Y. Sun, "Cyber-attacks detection in industrial systems using artificial intelligence-driven methods," *International Journal of Critical Infrastructure Protection*, vol. 38, p. 100542, 2022.

- [18] M. Al-Dhaheeri, P. Zhang, and D. Mikhaylenko, "Detection of cyber attacks on a water treatment process," *IFAC-PapersOnLine*, vol. 55, no. 6, pp. 667–672, 2022, 11th IFAC Symposium on Fault Detection, Supervision and Safety for Technical Processes SAFEPROCESS 2022.
- [19] D. T. Ha, N. X. Hoang, N. V. Hoang, N. H. Du, T. T. Huong, and K. P. Tran, "Explainable anomaly detection for industrial control system cybersecurity," *IFAC-PapersOnLine*, vol. 55, no. 10, pp. 1183–1188, 2022, 10th IFAC Conference on Manufacturing Modelling, Management and Control MIM 2022.
- [20] Z. Wu, S. Pan, G. Long, J. Jiang, X. Chang, and C. Zhang, "Connecting the dots: Multivariate time series forecasting with graph neural networks," in *Proceedings of the 26th ACM SIGKDD International Conference on Knowledge Discovery and Data Mining*, 2020, pp. 753–763.
- [21] B. Yu, H. Yin, and Z. Zhu, "Spatio-temporal graph convolutional networks: A deep learning framework for traffic forecasting," in *Proceedings of the 27th International Joint Conference on Artificial Intelligence (IJCAI)*, 2018, pp. 3634–3640.
- [22] A. Vaswani, N. Shazeer, N. Parmar, J. Uszkoreit, L. Jones, A. N. Gomez, Ł. Kaiser, and I. Polosukhin, "Attention is all you need," in *Advances in Neural Information Processing Systems (NeurIPS)*, vol. 30, 2017.
- [23] H. Zhou, S. Zhang, J. Peng, S. Zhang, J. Li, H. Xiong, and W. Zhang, "Informer: Beyond efficient transformer for long sequence time-series forecasting," in *Proceedings of the AAAI Conference on Artificial Intelligence (AAAI)*, 2021, pp. 11 106–11 115.
- [24] H. Ren, B. Xu, Y. Wang, C. Yi, X. Huang, J. Kou, T. Xing, M. Yang, J. Tong, and Q. Zhang, "Time-series anomaly detection service at Microsoft," in *Proceedings of the 25th ACM SIGKDD International Conference on Knowledge Discovery and Data Mining*, 2019, pp. 3009–3017.
- [25] J. Liu *et al.*, "TFANet: Time-frequency awareness network for industrial systems," *Sensors*, vol. 24, no. 18, 2024.
- [26] B. Boashash, "Estimating and interpreting the instantaneous frequency of a signal," *Proceedings of the IEEE*, vol. 80, no. 4, pp. 520–538, 1992.
- [27] P. Veličković, G. Cucurull, A. Casanova, A. Romero, P. Liò, and Y. Bengio, "Graph attention networks," in *International Conference on Learning Representations (ICLR)*, 2018.
- [28] D. Li, D. Chen, L. Shi, B. Jin, J. Goh, and S.-K. Ng, "MAD-GAN: Multivariate anomaly detection for time series data with generative adversarial networks," in *International Conference on Artificial Neural Networks (ICANN)*. Springer, 2019, pp. 703–716.
- [29] L. Ruff, R. A. Vandermeulen, N. Görnitz, L. Deecke, S. A. Siddiqui, A. Binder, E. Müller, and M. Kloft, "Deep one-class classification," in *International Conference on Machine Learning (ICML)*, 2018, pp. 4393–4402.
- [30] B. Zong, Q. Song, M. R. Min, W. Cheng, C. Lumezanu, D.-k. Cho, and H. Chen, "Deep autoencoding gaussian mixture model for unsupervised anomaly detection," in *International Conference on Learning Representations (ICLR)*, 2018.
- [31] D. Park, Y. Hoshi, and C. C. Kemp, "A multimodal anomaly detector for robot-assisted feeding using an LSTM-based variational autoencoder," *IEEE Robotics and Automation Letters*, vol. 3, no. 3, pp. 1544–1551, 2018.
- [32] L. Shen, Z. Li, and J. T. Kwok, "Timeseries anomaly detection using temporal hierarchical one-class network," in *Advances in Neural Information Processing Systems (NeurIPS)*, vol. 33, 2020.
- [33] M.-L. Shyu, S.-C. Chen, K. Sarinnapakorn, and L. Chang, "A novel anomaly detection scheme based on principal component classifier," in *Technical Report, University of Miami, Dept. of Electrical and Computer Engineering*, 2003.
- [34] C. C. Aggarwal, *Outlier Analysis*, 2nd ed. Springer, 2015.